Eur. Phys. J. AP **9**, 89–95 (2000)

THE EUROPEAN PHYSICAL JOURNAL APPLIED PHYSICS

Temperature dependence of the flow stress and the strain rate sensitivity at the transition from the Peierls mechanism to pinning by localized obstacles

B.V. Petukhov[1,a], M. Bartsch[2], and U. Messerschmidt[2]

[1] Institute of Crystallography, Russian Academy of Sciences, Leninskii Prospect 59, Moscow 117333, Russia
[2] Max Planck Institute of Microstructure Physics, Weinberg 2, Halle/Saale 06120, Germany

Received: 19 June 1999 / Revised: 22 July 1999 / Accepted: 5 October 1999

Abstract. Barriers of very different character such as localized obstacles and the extended Peierls- Nabarro relief may control the dislocation motion in crystals in different stress and temperature ranges. The great difference in the microscopic parameters characterizing these two mechanisms, *e.g.*, in the activation volumes, manifests itself even on the macroscopic scale as a strong change of the plastic properties in a rather narrow transition range of the temperature. A theory describing the temperature dependence of the flow stress and the strain rate sensitivity near the transition has been developed and compared with experimental data on the plastic deformation of cubic ZrO_2 single crystals in a soft orientation.

PACS. 61.70.G Dislocations: theory – 62.20.Fe Deformation and plasticity (including yield, ductility, and superplasticity)

1 Introduction

During the plastic deformation of crystalline materials, the dislocation motion is impeded by barriers of different nature: local obstacles like impurities, intrinsic point defects or small clusters, extended barriers like the potential relief of the crystal lattice (the Peierls-Nabarro relief), and long-range internal stress fields created by other dislocations. All these barriers contribute to the flow stress of the crystal in different ways. For the combined potential relief, the mechanism controlling the flow stress may change in different stress and temperature ranges, leading to certain peculiarities of the plasticity of the material in the transition range.

There are different separate models of the flow stress for each type of the individual barriers. For example, for the Peierls-Nabarro relief there exists a well elaborated theory allowing the calculation of the temperature dependence of the flow stress on the basis of the kink mechanism (for a review see, *e.g.*, [1,2]). For impure crystals or solid solutions there are detailed theories of solid solution hardening (*e.g.*, [3–5]). While the formal approach, which is frequently used to consider a combined potential relief, consists in calculating separate contributions of the different kinds of barriers and adding them up to the total flow stress, we shall rather treat the microscopic features of the mechanisms of dislocation motion and their transformation between the different stress and temperature ranges. Thus, it is the aim of the present paper to provide a description of the peculiarities of the plastic deformation based on a consistent physical concept of the dislocation dynamics in the combined potential relief formed by the joint action of the Peierls-Nabarro relief and localized obstacles as first considered in [6].

Hence, the stress dependence of the activation energy $\Delta G(\tau^*)$ appearing in the Arrhenius law of the dislocation velocity v

$$v = v_0 \exp\{-\Delta G(\tau^*)/kT\} \tag{1}$$

will be calculated. Here, T is the temperature, k is the Boltzmann constant, v_0 is a preexponential factor, and τ^* is the effective shear stress, describing the temperature dependent part of the flow stress. It is the difference between the applied shear stress $\tau_{\rm appl}$ and the long-range internal stress $\tau_{\rm i}$

$$\tau^* = \tau_{\rm appl} - \tau_{\rm i}. \tag{2}$$

The macroscopic plastic strain rate $\dot{\varepsilon}$ will be described, as usual, by using the Orowan relation

$$\dot{\varepsilon} = \rho b v = \dot{\varepsilon}_0 \exp\{-\Delta G(\tau^*)/kT\}, \tag{3}$$

where $\dot{\varepsilon}_0 = \rho b v_0 . \rho$ is the density of mobile dislocations, and b is the absolute value of the Burgers vector.

The theory presented here describes the drastic change of the strain rate sensitivity of cubic ZrO_2 single crystals

[a] e-mail: petukhov@ns.crys.ras.ru

observed in a narrow temperature range near the transition temperature $T_{\rm tr} = 750$ K manifesting the change of the micromechanisms controlling the dislocation motion.

2 Transition of the mechanisms controlling the dislocation motion

The localized obstacles and the extended Peierls-Nabarro relief play different roles in the process of dislocation motion. Localized obstacles divide the dislocations into segments, which advance by an independent kink generation along them. Because of the relatively short dislocation segments, the travel time of a kink along the dislocation is short compared to the waiting time of a kink pair nucleation. As discussed in more detail in [6,7], a specific mixed mode of the dislocation motion is operative in the combined potential relief. The elementary steps of the process are as follows. After a dislocation segment has reached a significant value of the bowing-out, one of the localized obstacles pinning the segment is overcome. The dislocation encounters other obstacles and becomes repinned again. If the temperature is high, the kink generation rate is high, too, and the time for the dislocation segment to bow out up to its maximum position is small compared with the time of overcoming the localized obstacles. In this temperature range, the mechanism controlling the flow stress is the overcoming of the local obstacles. With decreasing temperature, the kink generation rate also decreases. As soon as it becomes equal to the rate of overcoming the localized obstacles, a transition occurs of the mechanisms governing the dislocation motion. In a simplified quantitative way, the condition of the transition is met if the activation energies $\Delta G_{\rm l}(\tau^*)$ of overcoming localized obstacles and $\Delta G_{\rm P}(\tau^*)$ the Peierls mechanism are equal:

$$\Delta G_{\rm l}(\tau^*) \cong \Delta G_{\rm P}(\tau^*). \tag{4}$$

Here, differences in the preexponential factors of both processes are neglected.

The plasticity of cubic ZrO_2 at temperatures higher than the transition temperature $T_{\rm tr}$ has been described quantitatively in [8] using the local pinning model. It is the aim of the present paper to develop a description of the plastic deformation in the low-temperature range of $T < T_{\rm tr}$, where the kinetics of overcoming the Peierls-Nabarro barriers by the formation of kink pairs is essential.

The kink mechanism is well elaborated to describe the mechanical properties of sufficiently perfect crystals in which kinks are generated on long straight dislocations. However, in crystals containing local defects, which pin the dislocations, the conditions for the kink generation are changed. In the following sections, the peculiarities of the kink generation will be studied on dislocation segments bowing out between localized obstacles by the action of an external stress.

3 Kinetics of kink generation on bowed-out dislocation segments

First, the mechanical equilibrium states will be described of the bowed-out dislocation segments in the Peierls-Nabarro relief and their energetic characteristics. In the line tension approximation, the energy E of a curved dislocation configuration is described by the expression (see, *e.g.*, [2])

$$E = \int \left[\frac{\kappa}{2} \left(\frac{{\rm d}y}{{\rm d}x} \right)^2 + U_{\rm P} - \tau b y \right] {\rm d}x, \tag{5}$$

where $y(x)$ is the dislocation displacement at the point x along the dislocation, κ is the line tension, $U_{\rm P}(y)$ is the periodic Peierls-Nabarro potential, and τ is the acting stress component. For brevity, τ^* is replaced by τ in the theoretical part of the paper. The equilibrium configurations of the dislocation are obtained by minimising the energy in (5), *i.e.*

$$\frac{{\rm d}E}{{\rm d}y} = -\kappa \frac{{\rm d}^2 y}{{\rm d}x^2} + \frac{{\rm d}U_{\rm P}}{{\rm d}y} - \tau b = 0. \tag{6}$$

The first integral of equation (6) is

$$\frac{\kappa}{2} \left(\frac{{\rm d}y}{{\rm d}x} \right)^2 - U_{\rm P}(y) + \tau b y = {\rm const}. \tag{7}$$

The integration constant is determined from the bowing height h of the dislocation segment between the pinning points, which corresponds to the condition ${\rm d}y/{\rm d}x = 0$ at $y = h$. Therefore, const $= -U_{\rm P}(h) + \tau b h$. Solutions of equation (6) are obtained in the form

$$x = \pm \sqrt{\frac{\kappa}{2}} \int_y^h \frac{{\rm d}y'}{\sqrt{U_{\rm P}(y') - U_{\rm P}(h) + \tau b (h - y')}} \cdot \tag{8}$$

Here, h is an integration constant determined by the condition that the dislocation segment of length l is pinned at its ends: $x = 0$ $y = h$; $x = \pm l/2$ $y = 0$, *i.e.*, according to equation (8),

$$l = \sqrt{2\kappa} \int_0^h \frac{{\rm d}y'}{\sqrt{U_{\rm P}(y') - U_{\rm P}(h) + \tau b (h - y')}} \cdot \tag{9}$$

Inserting solution (8) into equation (5) yields the next quadrature expression for the energy of equilibrium configurations

$$E = 2 \int_0^h \sqrt{2\kappa [U_{\rm P}(y) - U_{\rm P}(h) + \tau b (h - y)]} {\rm d}y + [U_{\rm P}(h) - \tau b h] l. \tag{10}$$

While in crystals with a negligible Peierls-Nabarro relief there exists only one equilibrium configuration of the dislocation segment bowed under the action of the stress, a sufficiently high Peierls-Nabarro relief changes the situation qualitatively. From physical considerations one may

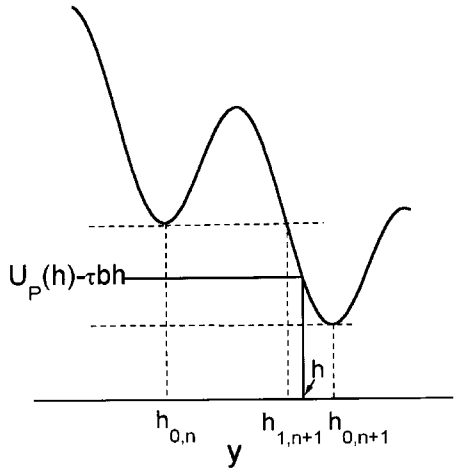

Fig. 1. Inclined potential profile $U_{\rm P}(y) - \tau by$, and illustration of forbidden ($h_{0,n} \div h_{1,n+1}$) and allowed values ($h_{1,n+1} \div h_{0,n+1}$) of equilibrium bowing heights h of a dislocation segment.

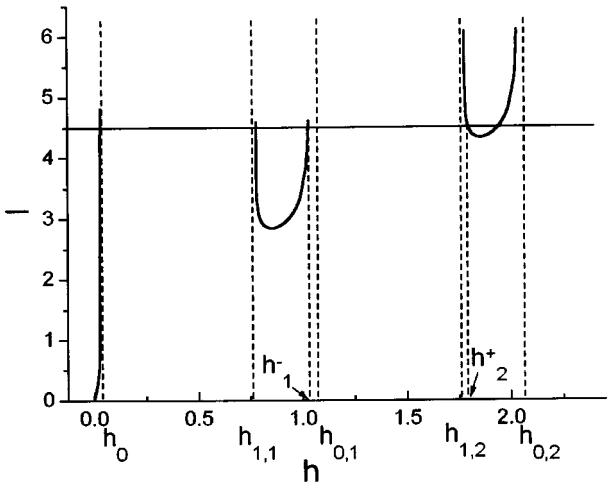

Fig. 2. Relationship between the dislocation segment length l and the equilibrium bowing h, illustrating the solution of equation (9) for the first three valleys of the Peierls-Nabarro relief. The calculation is made for the harmonic Peierls-Nabarro potential and a stress of $\tau = 0.1\tau_{\rm P}$. h is normalized by a, and l by the kink width $\sqrt{\frac{\kappa a}{2\pi\tau_{\rm P} b}}$.

expect that many locally stable (or metastable) configurations of the dislocation segment will exist, with tops resting in different valleys of the oscillating Peierls-Nabarro relief. Let us investigate this question more thoroughly.

The value of h corresponds to the maximum bowing of the dislocation segment between its pinning points. Those values of h for which equation (9) has a physical meaning are determined by the requirement that the expression under the root in equation (9) is not negative over the whole interval of $0 < y < h$, or, in other words, that the inclined potential $U_{\rm P}(y) - \tau by$ does not intersect the constant level $U_{\rm P}(h) - \tau bh$. Therefore, as it is evident from Figure 1, possible values of h are confined by intervals $h_{1,n+1} < h < h_{0,n+1}$, where n is the number of the valley in the Peierls-Nabarro relief. $h_{0,n}$ and $h_{1,n+1}$ are boundary values corresponding to the degeneration conditions $U_{\rm P}(h_{0,n}) - \tau bh_{0,n} = U_{\rm P}(h_{1,n+1}) - \tau bh_{1,n+1}$ (see Fig. 1). $h_{0,n}$ are points of minima of the potential, and $h_{1,n+1}$ are points corresponding to the same level of the potential. At $y \to h_{0,1n+1}$ the denominator of the integrand in equation (9) approaches zero, and the integral itself goes to infinity. Thus, the dependence of the right side of equation (9) on h looks as plotted schematically in Figure 2. In general, one can easily see that equation (9), for a fixed segment length, can have a number of solutions for h corresponding to the Peierls- Nabarro valleys for which minima of the function depicted in Figure 2 do not exceed the level l. Therefore, a number of equilibrium configurations may exist. One respective set of configurations is illustrated in Figure 3. Each of them yields an extreme in the energy relief of equation (5). It follows from Figure 2, illustrating the solution of equation (9), that there exist pairs of equilibrium configurations with tops in the same Peierls-Nabarro valley (except the first valley, where only one such configuration exists). One of these configurations corresponds to a minimum of the energy relief in equation (5), which is a stable one. Another configuration, which is an unstable saddle point configuration, corresponds to the top of the barrier dividing neighbouring minima. Configurations of the dislocation segment with an extended flat top correspond to the values of h which are close to the boundary values $h_{0,n}$. The configurations of types $1'$ to $5'$ in Figure 3 correspond to those values of h which are close to $h_{1,n}$. It is expected and confirmed by numerical calculations that configurations with the flat top are stable, whereas the configurations of types $1'$ to $5'$, which are analogous to an ordinary kink pair on a rectilinear dislocation, are unstable and correspond to states on tops of barriers separating different minima in the energy relief of equation (5).

In order to describe the kinetics of the thermal activation of the motion of a dislocation segment one has to calculate the activation energies for transitions between subsequent stable dislocation states. A respective procedure may be as follows. For a given segment length l, equation (9) is solved yielding the values h_n^- and h_{n+1}^+ corresponding to the stable configuration in the nth Peierls-Nabarro valley and to the saddle point configuration at the top of a barrier, separating the states of the dislocation segment in the nth and $(n+1)$th valleys. Then, using equation (10) yields the difference $\Delta G_{\rm P}^n$ of the energies of these two configurations

$$\Delta G_{\rm P}^n = \int_0^{h_{n+1}^+} \sqrt{8\kappa[U_{\rm P}(y) - U_{\rm P}(h_{n+1}^+) + \tau b(h_{n+1}^+ - y)]}\,{\rm d}y - \int_0^{h_n^-} \sqrt{8\kappa[U_{\rm P}(y) - U_{\rm P}(h_n^-) + \tau b(h_n^- - y)]}\,{\rm d}y + [U_{\rm P}(h_{n+1}^+) - U_{\rm P}(h_n^-) - \tau b(h_{n+1}^+ - h_n^-)]l. \quad (11)$$

This expression is the required modification of the well-known formula for the kink pair formation energy on a

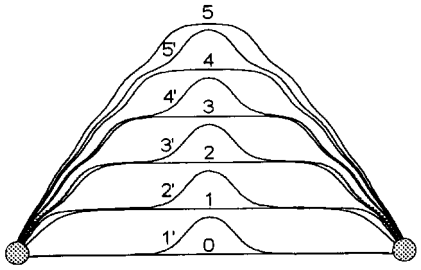

Fig. 3. Stable equilibrium configurations (0 to 5) and unstable ones ($1'$ to $5'$ on the top of the separating barrier) of the dislocation segment in different valleys of the Peierls-Nabarro relief. $l = 17\sqrt{\frac{\kappa a}{2\pi\tau_{\rm P} b}}$, $\tau = 0.1\tau_{\rm P}$.

rectilinear dislocation [9]

$$\Delta G_{\rm P0}(\tau) = \int_{h^-}^{h+} \sqrt{8\kappa[U_{\rm P}(y) - U_{\rm P}(h^+) + \tau b(h^+ - y)}\,{\rm d}y. \tag{12}$$

For a sufficiently large length l, the solutions of equation (9) h_n^- are close to the points of the minima $h_{0,n}$ of the potential $U_{\rm P}(y) - \tau by$ and the solutions h_{n+1}^+ are close to the conjugating points $h_{1,n+1}$ corresponding to the same level of the potential $U_{\rm P}(h_n^-) - \tau b h_n^- = U_{\rm P}(h_{n+1}^+) - \tau b h_{n+1}^+$. As one can easily see, $\Delta G_{\rm P}^n$ in equation (11) then turns to $\Delta G_{\rm P0}(\tau)$ of equation (12) with $h^- = h_n^-, h^+ = h_{n+1}^+$, which, in fact, does not depend on n owing to the periodicity of $U_{\rm P}(y)$.

In the general case of an arbitrary finite segment length, the heights of barriers $\Delta G_{\rm P}^n$ depend on the curvature of the segment, which increases with increasing bowing characterized by the value of n. The case of large $n (n \gg 1)$ and low stresses compared to the Peierls stress $\tau_{\rm P}$ is of special interest, as the description can be simplified and the qualitative difference arising from considering the Peierls-Nabarro relief is more evident.

4 Activation parameters for low stresses compared to the Peierls stress

For stresses which are low compared to the Peierls stress $\tau_{\rm P}$, the expansion of equation (11) for small τ yields a simplified analytic form for the stress dependence of the barrier height $\Delta G_{\rm P}^n$

$$\Delta G_{\rm P}^n \approx 2E_k + \tau ba\sqrt{\frac{\kappa}{U_{\rm P}''}}\left\{\ln(1+\sqrt{1-M}) + (1-\sqrt{1-M})\right.$$
$$\left.\times\left[\sqrt{2} - \ln((\sqrt{2}-1)M)\right] - \sqrt{1-M}\left(\ln\frac{U_{\rm P}'' a}{\tau b} + \sqrt{2U_{\rm P}''}J + 1\right)\right\}. \tag{13}$$

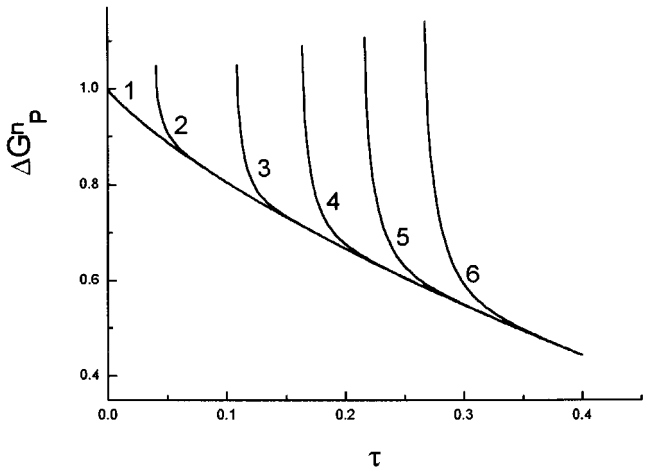

Fig. 4. Heights of the energy barriers between equilibrium states of the dislocation segment in valleys of the Peierls-Nabarro relief with different numbers n for the low stress range, equation (13). Curve 1 presents the stress dependence of the energy of the kink pair formation on an extended straight dislocation according to the ordinary model (equation (15)), the other curves correspond to $2: n = 4$; $3: n = 6$; $4: n = 8$; $5: n = 10$; $6: n = 12$. $l = 50\sqrt{\frac{\kappa a}{2\pi\tau_{\rm P} b}}$.

Here,

$$M = \left(\frac{4a}{h_0}\right)^2 \exp\left\{-\sqrt{\frac{U_{\rm P}''}{\kappa}}\left(l - \sqrt{\frac{8Kna}{\tau b}}\right.\right.$$
$$\left.\left. + \frac{2E_k}{\tau ba} - 2\sqrt{2\kappa}J\right)\right\}, \tag{14}$$

with

$$J = \int_0^a \frac{{\rm d}y}{a}\left\{\frac{y}{\sqrt{U_{\rm P}(y)}} - \sqrt{\frac{2}{U_{\rm P}''}}\frac{a}{(a-y)}\right\}$$

and $U_{\rm P}'' = {\rm d}^2 U_{\rm P}(0)/{\rm d}y^2$.

The obtained general expression (13) allows one to calculate the activation parameters characterizing the relaxation kinetics of the dislocation segment for different physical situations. For a small bowing, *i.e.* small values of n, the curved part of the segment is relatively short, and most part of the segment is almost straight. In such a situation, the saddle point configuration is similar to the ordinary configuration, with a critical kink pair in the homogeneous case (on an extended straight dislocation). In this case $M \approx 0$, and $\Delta G_{\rm P}^n$ corresponds to the approximate expression for the activation energy of a kink pair $\Delta G_{\rm P0}(\tau)$ at low stresses (see, *e.g.*, [10])

$$\Delta G_{\rm P}^n = \Delta G_{\rm P0}(\tau)$$
$$\approx 2E_k - \tau ba\sqrt{\frac{\kappa}{U_{\rm P}''}}\left\{\ln\frac{U_{\rm P}'' a}{2\tau b} + \sqrt{2U_{\rm P}''}J + 1\right\}. \tag{15}$$

E_k is the formation energy of a single kink. For the particular case of the harmonic Peierls- Nabarro potential

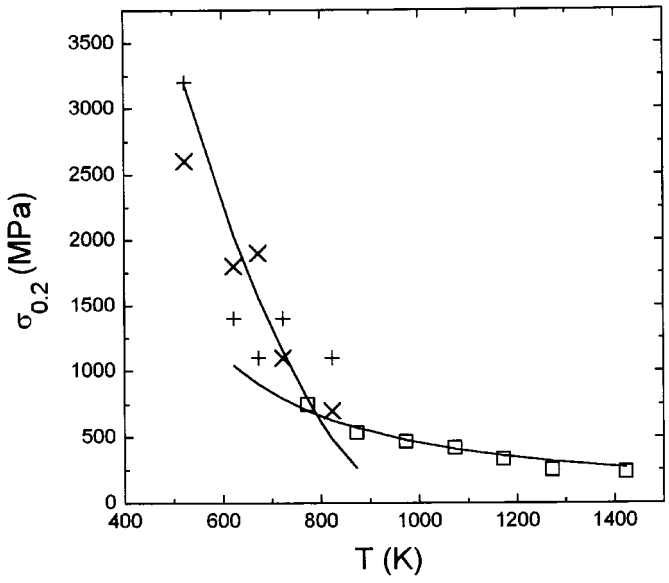

Fig. 5. Temperature dependence of the flow stress of cubic ZrO_2. The symbols represent experimental data: 11 mol% Y_2O_3, $\dot{\varepsilon} = 10^{-6}s^{-1}$, data from [7,12,13]; +12,6 mol% Y_2O_3 [14,15], × 9.4 mol% Y_2O_3 [14,15], $\dot{\varepsilon} = 2 \times 10^{-4}s^{-1}$. The curves are the theoretical predictions of the modified kink mechanism at low temperatures and of local obstacles at higher temperatures.

$U_P(y) = (\tau_P ab/2\pi)(1 - \cos(2\pi y/a))$, this expression takes the form

$$\Delta G_{P0}(\tau) \approx 2E_k \left[1 - \frac{\pi}{8}\frac{\tau}{\tau_P}\left(\ln\left(\frac{16\tau_P}{\pi\tau}\right) + 1\right)\right], \quad (16)$$

where

$$E_k = \left(\frac{2}{\pi}\right)^{3/2} \sqrt{\kappa\tau_P ba^3}.$$

The stress dependence of the height of the barriers between the different states of the bowed-out dislocation segment is illustrated in Figure 4. There are several branches of this function corresponding to the numbers of the Peierls-Nabarro valleys. Their deviations from the stress dependence for the ordinary kink pair generation (curve 1) become pronounced when, with decreasing stress, the bowing of the dislocation segment approaches the limit of allowed values. The dependencies are cut off at certain critical stresses, below which equilibrium configurations of the dislocation segment with a corresponding value of n do not exist.

5 Flow stress and strain rate sensitivity in the transition temperature range

As mentioned in Section 2, for a continuous dislocation motion at stresses above the transition stress the rates of overcoming the Peierls-Nabarro barriers and the localized obstacles are equal so that equation (4) is fulfilled. This means that obstacles, which pin the segment, are overcome with a very high probability when the bowing reaches a sufficiently high value to reduce the height of the local barrier $\Delta G_l(\tau)$ to the required level. This condition fixes the value of bowing which is decisive for determining the dislocation velocity. In the case when $\Delta G_l(\tau)$ is large in comparison to the kink pair energy $2E_k$, this bowing should also be large and close to the value of the the mechanical breakaway from the obstacles without thermal activation. A simple estimation of this value of bowing, pointed out in [11], is $na = f_c^2/8\kappa\tau b$, where f_c is a critical value of the force the dislocation segment exerts on the local obstacle (the obstacle strength).

With this value of na, M in equation (14) is transformed into the following form

$$M = \left(\frac{4a}{h_0}\right)^2 \times \exp\left\{-\sqrt{\frac{U_P''}{\kappa}}\left(l + \frac{(2E_k - f_c a)}{\tau ba} - 2\sqrt{2\kappa}J\right)\right\}. \quad (17)$$

Inserting this modified M into equation (13), we obtain the stress dependence of the barrier height ΔG_P^c for the continuous dislocation motion.

Let us calculate also the activation volume V, which corresponds to the barrier height ΔG_P^c

$$V = -\frac{d\Delta G_P^c}{d\tau} = \frac{f_c a - 2E_k}{\tau}\left\{\frac{1}{2}\frac{M}{\sqrt{1-M}} \times \left[\sqrt{2} + 1 + \sqrt{2U_P''}J - \ln\left(\left(\sqrt{2}-1\right)M\frac{\tau b}{U_P'' a}\right)\right] - \frac{1}{2}\frac{M}{\sqrt{1-M}+1-M} + \sqrt{1-M} - 1\right\} - ba\sqrt{\frac{\kappa}{U_P''}}\left\{\ln\left(1+\sqrt{1-M}\right) + \left(1-\sqrt{1-M}\right) \times \left[\sqrt{2} - \ln\left(\left(\sqrt{2}-1\right)M\right)\right] - \sqrt{1-M}\left(\ln\frac{U_P'' a}{\tau b} + \sqrt{2U_P''}J\right)\right\}. \quad (18)$$

6 Experimental results and comparison with the model

The experimental data are described in more detail elsewhere [7,12,13]. This paper is restricted to a short summary of results, which are necessary for a comparison with the theoretical model. Cubic ZrO_2 single crystals stabilized with 11 mol% Y_2O_3 were compressed along the $[1\bar{1}2]$ direction. This orientation activates the primary $[1\bar{1}0](001)$ slip system with an orientation factor of $m = 0.47$. The experiments were carried out in an

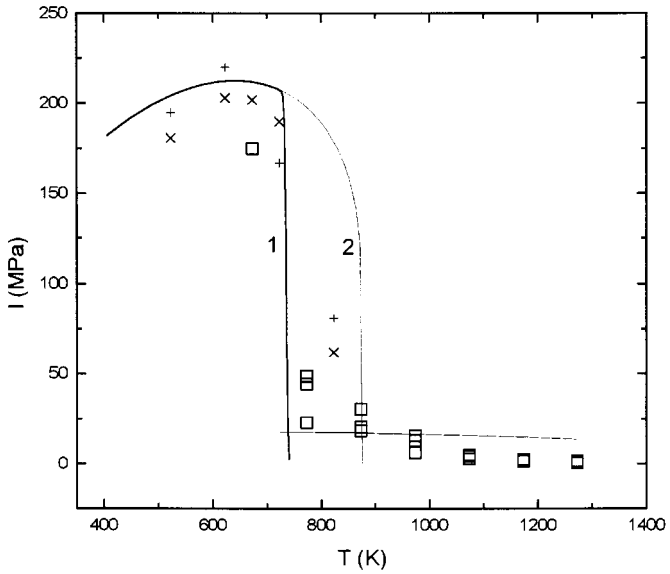

Fig. 6. Strain rate sensitivity of cubic ZrO_2 as a function of temperature. Curve 1 shows the theoretical dependence of the modified kink mechanism, curve 2 shows the strain rate sensitivity of the ordinary kink mechanism. Symbols and references as in Figure 5.

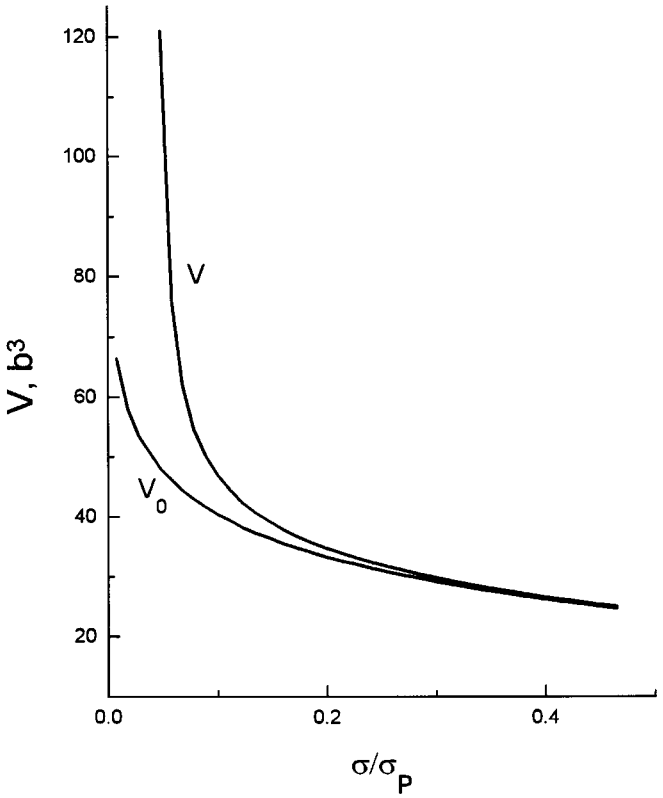

Fig. 7. Stress dependence of the activation volume for the ordinary (V_0) and the modified (V) kink mechanisms.

INSTRON 8586 testing machine in air between 673 K and 873 K. Figure 5 is a plot of the flow stress $\sigma_{0.2}$ at a plastic strain of 0.2% *versus* the temperature (σ is the applied (compression) stress, which is related to the shear stress *via* the orientation factor according to $\tau = m\sigma$). In order to obtain the strain rate sensitivity, strain rate cycling and stress relaxation experiments were performed. Figure 6 presents the strain rate sensitivity $I = \mathrm{d}\sigma/\mathrm{dln}\dot{\varepsilon}$ *versus* the temperature. In Figures 5 and 6 also data measured under confining hydrostatic pressure [14,15] are shown.

Combining the Orowan relation and equation (3)

$$\Delta G_{\mathrm{P}}^{\mathrm{c}}(\tau^*) = kT\ln(\dot{\varepsilon}_0/\dot{\varepsilon}) \tag{19}$$

allows one to calculate the temperature dependence of the flow stress $\tau_{\mathrm{appl}}(T) = \tau^* + \tau_{\mathrm{i}}$. The internal stresses τ_{i} can be estimated from the dislocation density by a formula [12] for Taylor hardening

$$\tau_{\mathrm{i}} = \alpha K b F_{\mathrm{m}} \rho^{1/2}/2\pi. \tag{20}$$

Here, α is a numerical constant of about 8, K is the energy factor of screw dislocations (80 GPa at 873K), and $F_{\mathrm{m}} = 0.3$ is a normalized maximum interaction force between parallel dislocations on {100} planes. The dislocation density within the slip bands has been counted from transmission electron micrographs. The temperature dependence of the obtained internal stresses can be approximated by an empirical formula

$$\tau_{\mathrm{i}} = 42\ \mathrm{MPa} + 58.2\ \mathrm{MPa} \times \exp\left\{(787 - T[\mathrm{K}])/135.6\right\}. \tag{21}$$

Formulae (13), (17) and (19) were used to describe the experimental data for the flow stress in Figure 5. The strain rate sensitivity I was estimated according to

$$I = \Delta\sigma/\Delta\ln\dot{\varepsilon} = kT/(mV), \tag{22}$$

where the activation volume V is described by formula (18). At temperatures below the transition range, the smooth temperature dependence of the shear modulus may be neglected in comparison to the strong temperature dependence of the flow stress. For the range above the transition temperature, where the temperature sensitivity of the flow stress decreases, our description follows the calculations of the paper [8] taking into account the temperature dependence of the shear modulus. The parameters τ_{P}, E_k, f_{c}, and l were determined by fitting the theoretical formulae to the experimental data of Figures 5 and 6, yielding $\tau_{\mathrm{P}} = 4500$ MPa, $E_k = 0.9$ eV, $f_{\mathrm{c}} = 6.3E_k/a$, and $l = 100\ b$. In Figures 5 and 6, the results of the fitting are shown as full lines. The calculated curves represent satisfactorily the temperature dependence of the flow stress and the steep drop of the strain rate sensitivity at $T \approx 750$ K. The curves for $T > 750$ K in the figures reproduce the description suggested in [8] based on the local pinning model. The data of [14,15] agree quite well with those of the present authors in the small range of overlap. The localized obstacles are most probably small precipitates. The pinning is evidenced by mechanical transmission electron microscopy. The parameters of these obstacles are discussed in [7]. The obstacle distance of $l = 100\ b$ corresponds to the measurements

from electron micrographs at the high stress limit. Figure 7 shows the stress dependence of the activation volume with determined parameters for the modified kink mechanism in comparison to the ordinary one. It may be of interest to estimate the typical bowing height of the dislocation segments. Using the parameters in the transition range indicated above yields $n_c = h_c/a \approx 5$, the reasonable order of magnitude.

7 Conclusions

- A new model is suggested to describe the simultaneous action of the Peierls-Nabarro mechanism and localized obstacles in controlling the dislocation mobility.
- The model extends the preliminary qualitative formulation in [7] and gives formulae for the temperature dependence of the flow stress and its temperature sensitivity in the transition range between both mechanisms.
- The model is fitted to experimental data on the low-temperature deformation of cubic zirconia. This fitting confirms the values of parameters estimated in the previous study on the semi-qualitative basis. The new model yields also an improved description of the strong increase of the strain rate sensitivity with decreasing temperature in the transition range.

The research described in this publication was made possible in part by Grant INTAS 96-363.

References

1. J.P. Hirth, J. Lothe, *Theory of Dislocations* (Wiley, New York, 1982).
2. A. Seeger, P. Schiller, *Physical Acoustics, III A*, edited by W.P. Meson (Academic Press, New York and London, 1966), p. 361.
3. J. Friedel, *Dislocations* (Oxford, Pergamon, 1964).
4. E. Nadgorny, Progr. Mater. Sci. **31**, 1 (1988).
5. T. Suzuki, S. Takeuchi, H. Yoshinaga, *Dislocation Dynamics and Plasticity*, (Springer, Berlin, 1991).
6. B.V. Petukhov, Crystallog. Rep. **41**, 197 (1996).
7. B. Baufeld, B.V. Petukhov, M. Bartsch, U. Messerschmidt, Acta Mater. **46**, 3077 (1998).
8. B. Baufeld, M. Bartsch, U. Messerschmidt, D. Baither, Acta Metall. Mater. **43**, 1925 (1995).
9. V. Celli, M. Kabler, T. Ninomiya, T.R. Thomson, Phys. Rev. **131**, 58 (1963).
10. A. Seeger, Z. Metallk. **72**, 369 (1981).
11. L.P. Kubin, F. Louchet, D. Vesely, Philos. Mag. A **39**, 433 (1979).
12. U. Messerschmidt, B. Baufeld, D. Baither, in *Zirconia Engineering Ceramics: Old Challenges - New Ideas*, edited by E. Kisi (Key Eng. Mater. **153-154**, Trans. Tech. Publ., 1998), p. 143.
13. B. Baufeld, Doctoral thesis, Halle (Saale), 1996.
14. P. Teracher, H. Garem, J. Rabier, in *Strength of Metals and Alloys*, edited by D.G. Brandon, R. Chaim, A. Rosen (Freund Publs. London, 1991), p. 217.
15. P. Teracher, Ph.D. thesis, Poitiers, 1990.